Neuroradiology (2001) 43: 797–808

L.L. Chan
S. Manolidis
K. H. Taber
L. A. Hayman

Surgical anatomy of the temporal bone: an atlas

Received: 9 May 2000
Accepted: 20 July 2000

Invited Presentation at Radiological Society of North America, 1999

L.L. Chan · K. H. Taber · L. A. Hayman (✉)
Department of Radiology,
Baylor College of Medicine,
One Baylor Plaza,
Houston TX 77030–3498, USA
e-mail: lhayman@bcm.tmc.edu
Tel.: + 1-713-798 5146
Fax: + 1-713-798 5745

L.L. Chan · K. H. Taber · L. A. Hayman
Herbert J. Frensley Center for Imaging Research, Baylor College of Medicine

S. Manolidis
Department of Otorhinolaryngology, Baylor College of Medicine

K.H. Taber · L. A. Hayman
Department of Psychiatry & Behavioral Sciences, Baylor College of Medicine

Abstract This atlas demonstrates the usefulness of reconstructed high-resolution CT for planning temporal bone surgery. The first part focuses on a sagittal plane, the second on a rotated longitudinal plane, and the third on a rotated transverse plane. We believe knowledge of temporal bone anatomy in these planes facilitates surgical planning by showing anatomic relationships and providing a customized map for each patient. This decreases the likelihood of surgical mishap and improves teaching.

Keywords Temporal bone · Computed tomography · Temporal bone surgery

Introduction

Temporal bone anatomy is complex [1, 2, 3, 4, 5]. Significant normal variations in the relationships between surgically critical structures have been documented by clinical and cadaver studies [6, 7, 8, 9, 10, 11, 12, 13]. These have shown that, although the inner ear structures have constant relationships, there are wide variations in the distances between the nerves and vessels, and their relationships to each other and to the inner ear [6, 7, 11]. There is therefore a need to provide the surgeon with easily understood, customized presurgical images which enable identification of potentially dangerous variations in anatomy. They should highlight the degree of pneumatization in critical areas, map the course of vessels and nerves, and locate the fissures [10, 11, 14, 15, 16]. To operate successfully on the temporal bone, the surgeon must have information in three planes (superoinferior, anteroposterior, and mediolateral).

Providing the surgeon with the required data – and showing pathology – are the goals of temporal bone im-

aging [4, 5, 17, 18]. However, technical limitations of CT resulted in the use of axial and coronal sections [19, 20, 21]. In the traditional high-resolution study, axial sections are used to define the anteroposterior and mediolateral, and coronal sections the superoinferior and mediolateral relationships. But axial sections show superoinferior relationships poorly, and the same is true of the coronal sections and the anteroposterior relationships. To overcome these deficiencies, some groups have suggested the addition of direct high-resolution CT (HRCT) [22, 23]. The images are difficult to reproduce because they require both a skilled technician and a cooperative patient; this technique has therefore not become common practice. Other groups have resorted to advanced technology and 3D volumetric rendering algorithms [24], combined with frameless image-guided navigation techniques [25, 26]. These require sophisticated software, expensive hardware, and a dedicated team of professionals. For instance, data transfer to a high-end workstation is necessary before time-intensive 3D reconstructions by interactive segmentation or thresholding can be undertaken. Hence, these solutions have also not found widespread use.

Axial sections have been used to reconstruct temporal bone anatomy in coronal and sagittal planes [23, 27]. We undertook this study to determine if a simple, practical imaging reformation protocol, suitable for displaying temporal bone surgical anatomy, could be developed using commonly available soft- and hardware. We looked at its usefulness in three areas: an inverted sagittal plane in planning a middle cranial fossa (MCF) approach to pathology in the internal auditory canal; a longitudinal plane, for the infratemporal (ITF) approach; and a transverse plane for the ITF and for the facial recess (FR) approaches.

Materials and methods

We scanned a normal temporal bone in vivo in the axial plane, parallel to the orbitomeatal line, with the following parameters: 120 kV, 350 mA, 1 mm slice thickness, no interslice gap, 512 × 512 matrix, bone algorithm. The data were transferred to a workstation via a standard computer network. We used the commercially available two-dimensional multiplanar reformation function to reformat the images in the planes selected, in 1 mm sections without an interslice gap, employing the maximum-intensity projection. We reviewed the reformatted images with an window width of 4000 Hounsfield units [21, 28].

The otology and neuroradiology staff assessed all images for practical utility and teaching value and sections containing vital information were chosen to construct the atlas. Image resolution was best at the workstation where the window settings could be adjusted to show soft tissue and thin bones, and then set for bone windows. Surgically important relationships were determined (Tables 1, 2, 3). Lists of anatomical structures were formulated and abbreviations were chosen to label the reformatted images [18]. For clarity, five structures (vestibule and superior semicircular canal (gold), internal carotid artery (red), facial nerve (green), cochlea (purple), and jugular fossa and sigmoid sinus (blue) are color-coded throughout (figures 1–7). The images are printed from lateral to medial, to further orient the surgeon.

Reconstructed images display temporal bone anatomy in the optimal plane of section and at sufficient resolution to be useful in planning the surgical approach. A batch of 30 reconstructed images can be easily reformatted on the workstation. The reconstructed images appear on the monitor within a minute with the click of a button, after the position of the plane of reformation has been defined.

The atlas

An inverted sagittal atlas for the MCF approach

For the sagittal plane the images were inverted to match the surgical perspective (Fig. 1) and labeled (Fig. 3) [18]. Several structures, while not relevant to the MCF approach, were well demonstrated in the sagittal reconstructions: the petrotympanic fissure (which contains the anterior tympanic artery and chorda tympani), vaginal plate of tympanic bone, second genu and vertical segment of the facial canal.

The images can be inverted and printed lateral-to-medial to further orient the surgeon. This can be especially useful for planning the MCF approach because the surgeon is most concerned with superoinferior relationships, which are condensed into a single sagittal view.

The advantages of this view for the MCF approach are discussed below. The approach is traditionally performed for preservation of hearing in patients with small acoustic schwannomas laterally in the internal auditory canal. It is also used for decompression of the facial nerve in Bell's palsy and to repair the nerve in traumatic facial paralysis. The surgeon sits at the patient's head and approaches the superior surface of the temporal bone (Fig. 1). The superoinferior relationships are therefore critical.

The best way to show the usefulness of the inverted sagittal images is to describe the surgery and illustrate each critical juncture and/or relationship using the data gathered in this study. The approach begins with a temporal craniotomy and exposure of the bony floor of the middle cranial fossa by elevation of the temporal lobe. The dura mater is then elevated to uncover the superior surface of the temporal bone (Fig. 1). The reader can use the sagittal images to locate the foramen spinosum (Fig. 3f), which contains the middle meningeal artery and marks the starting point for the dural dissection. The operation can be divided into two stages: finding, then unroofing the internal auditory canal. We describe each stage and its risks.

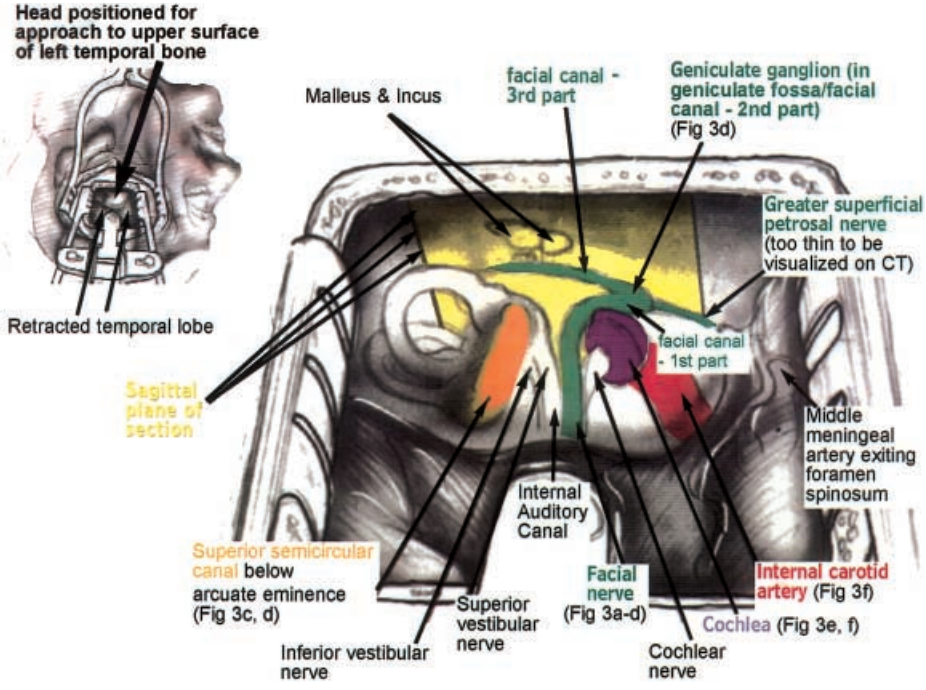

Fig. 1 Orientation of left temporal bone structures in middle cranial fossa (MCF) approach. Note surgeon's position with respect to temporal bone and how inverting the image to place the condyle of the mandible above the middle and posterior cranial fossae recreates the surgical perspective. The sagittal plane of section is marked by the yellow square lateral to the cochlea and vestibule. Note also two critical surgical landmarks for locating the internal auditory canal: the arcuate eminence (overlying the superior semicircular canal) and the foramen spinosum. Reproduced with modifications and permission from [61]

Finding the internal auditory canal

Two methods can be used independently or in combination. In the first, the surgeon searches for a distinct arcuate eminence (absent in 15 % of patients) [31]. This is delicately thinned until the fluid within the underlying superior semicircular canal can be seen as a bluish area, a process termed "blue lining" (Fig. 1). The surgeon can now find the internal auditory canal, which is predictably at a 60 ° angle to the plane of the superior semicircular canal. Inadvertent entry into the superior semicircular canal during blue lining will cause permanent deafness. The thickness of the bone over the superior semicircular canal has apparently not been reported. On our HRCT images this bone often appeared dehiscent, due to partial-volume artifacts (critical relationship 4, Table 1, Fig. 3 d). The surgeon should be alerted to this artifact and distinguish it from pneumatization of the bone overlying the superior semicircular canal which would cause difficulties finding the arcuate eminence and "blue lining".

The second method begins with identification of the foramen spinosum (Figs. 1, 3 f). The greater superficial petrosal nerve lies in proximity to this structure and can be followed back to the geniculate fossa (Fig. 3 d). Then the first genu (in the geniculate fossa) and labyrinthine segment of the facial nerve are exposed. This leads to exposure of the distal internal auditory canal (critical relationships 1, 2, 3, and 8, Table 1; Fig. 3 d, f). Inadvertent entry into the vestibule or cochlea, which underlie these structures, also causes immediate, permanent deafness. Identification of its various segments decreases the risk of injury to the facial nerve.

Unroofing the internal auditory canal

Following identification of the distal part, the entire canal can be defined as a prelude to opening its dura mater and identifying the 7–8th nerve complex (critical relationships 5 and 6, Table 1; Fig. 3 f). Imaging can alert the surgeon to extensive temporal bone pneumatization and show the number and depth of air cells which will be encountered prior to defining the underlying internal auditory canal. Inadvertent entry into the internal auditory canal can damage the facial or cochlear nerves by direct pressure or by interruption or spasm of the delicate vessels supplying these nerves. In some cases [32] the anterior inferior cerebellar artery is intimately related to the internal auditory canal, looping within it for a variable distance. Interruption or damage to this artery can have catastrophic results, causing a brain-stem infarct (the inferolateral pontine syndrome of Foville) [33].

The MCF approach can be widened to expose not only the internal auditory canal but the petrous apex, in the "extended MCF approach". The petrous internal carotid artery is skeletonized (critical relationship 7, Table 1; Fig. 3 f). Inadvertent opening of the artery at this point is catastrophic and usually lethal, because clipping of the petrous segment is technically difficult; when it can be accomplished, it may nevertheless result in a large cerebral infarct.

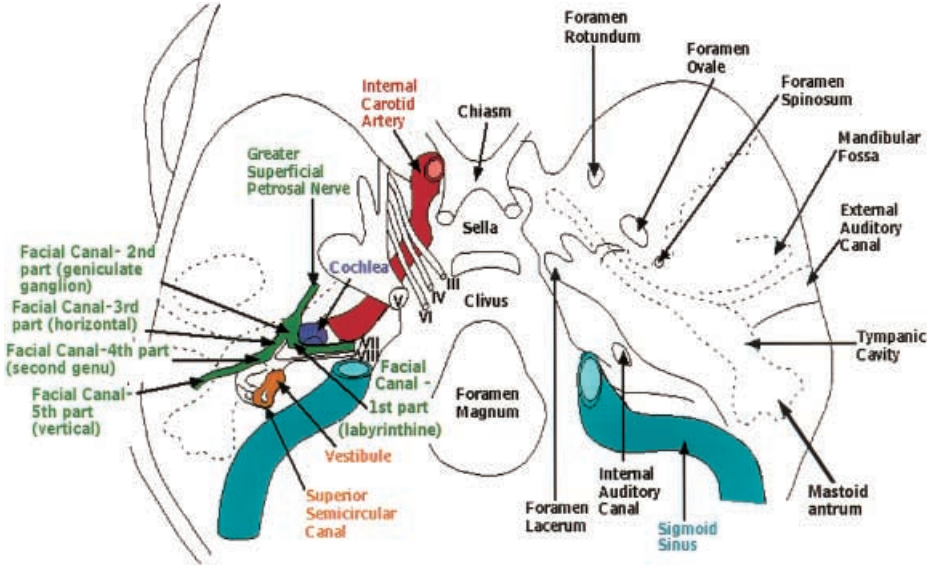

Fig. 2 Diagram of skull base from above identifies and color-codes vital structures shown in Figs. 1 and 3

Table 1 Critical surgical relationships, middle cranial fossa approach (Fig. 3)

1	Vestibule to geniculate fossa portion of facial canal
2	Vestibule to middle cranial fossa (shortest distance)
3	Vestibule to middle cranial fossa (vertical distance)
4	Superior semicircular canal to middle cranial fossa
5	Internal auditory canal to middle cranial fossa (shortest distance)
6	Internal auditory canal to middle cranial fossa (vertical distance
7	Internal carotid artery to internal auditory canal (shortest distance)
8	Foramen spinosum to basal turn of cochlea (shortest distance)

We considered two other landmarks: the tympanic segment of the facial canal and the horizontal portion of the petrous internal carotid artery. Both are, however, inconstant, because they depend upon the degree of pneumatization and other factors [8, 42]. In contrast, the otic capsule contained two constant structures in the transverse plane: the superior semicircular canal and the modiolus of the cochlea [8, 34, 35, 36, 39, 40, 41]. The superior semicircular canal was, therefore chosen since it could be most easily identified on the axial images, even by the technician. Thus, we constructed a

A rotated longitudinal atlas for the infratemporal approach (Figs. 4, 5)

This approach is performed for a variety of conditions such as glomus tumors, and other benign and malignant skull base tumors [34, 35]. The longitudinal projection provides the surgeon with an individualized map which can be used to judge the depth (ventrodorsal distances) between vital structures as the operation proceeds from the mastoid into the middle ear and beyond [36, 37, 38, 39]. We experimented with various planes of two-dimensional reformation to reproduce the surgical plane along the long axis of the petrous bone [39, 40]. The first landmark we considered for prescribing this plane was the posterior surface of the petrous bone, because it approximates to its long axis. However, we rejected it, because it was convex to the posterior cranial fossa with a variable apex formed by the porus acousticus; the angle it forms with the sagittal plane varies between individuals; and the angle also changes from the roof to the base in the same individual [13, 41].

Fig. 3 a–f Inverted sagittal reconstructed of left temporal bone ▶ place its superior aspect at bottom of image. Numbers (*1–8*) indicate surgical relationships (Table 1) discussed in text. *Insert* indicates distance from first section. **a.** Note malleus (*M*) and incus (*I*). Stylomastoid foramen (*smf*) leads into facial canal.(*FC5*). **b.** Note facial (*FC4*) and lateral semicircular (*LSC*) canals. Anterior portion of chorda tympani runs in canal of Huguier, in petrotympanic fissure (*PTF*). **c.** Note oval window (*ow*), vestibule (*V*), facial (*FC3*) and semicircular (*SSC, PSC, LSC*) canals. **d.** Note round window (*rw*) and geniculate fossa (*FC2*). Superior wall (*4*) of SSC appears dehiscent due to obliquity and volume averaging. **e.** Shows the cochlea (*C*), with its basal turn (*btC*) and fundus of internal auditory canal (*IAC*). **f.** Note IAC, btC, petrous internal carotid artery (*ICA*), jugular fossa (*JF*) and foramen spinosum (*fs*). Other abbreviations: *C* cochlea; *CM* condyle of mandible; *EAC* external auditory canal; *FC2–5* geniculate fossa, horizontal, second genu and vertical portions of facial canal; *fl* foramen lacerum; *I* incus; *JCS* jugulocarotid spine; *LSC* lateral semicircular canal; *M* malleus; *MCF* middle cranial fossa; *MF* mandibular fossa; *P* promontory; *PCF* posterior cranial fossa; *PSC* posterior semicircular canal; *rw* round window; *SP* styloid process; *sq* squamous temporal bone; *SS* sigmoid sinus; *SSC* superior semicircular canal; *TC* tympanic cavity; *tgT* tegmen tympani; *tt* tensor tympani; *VP* vaginal plate

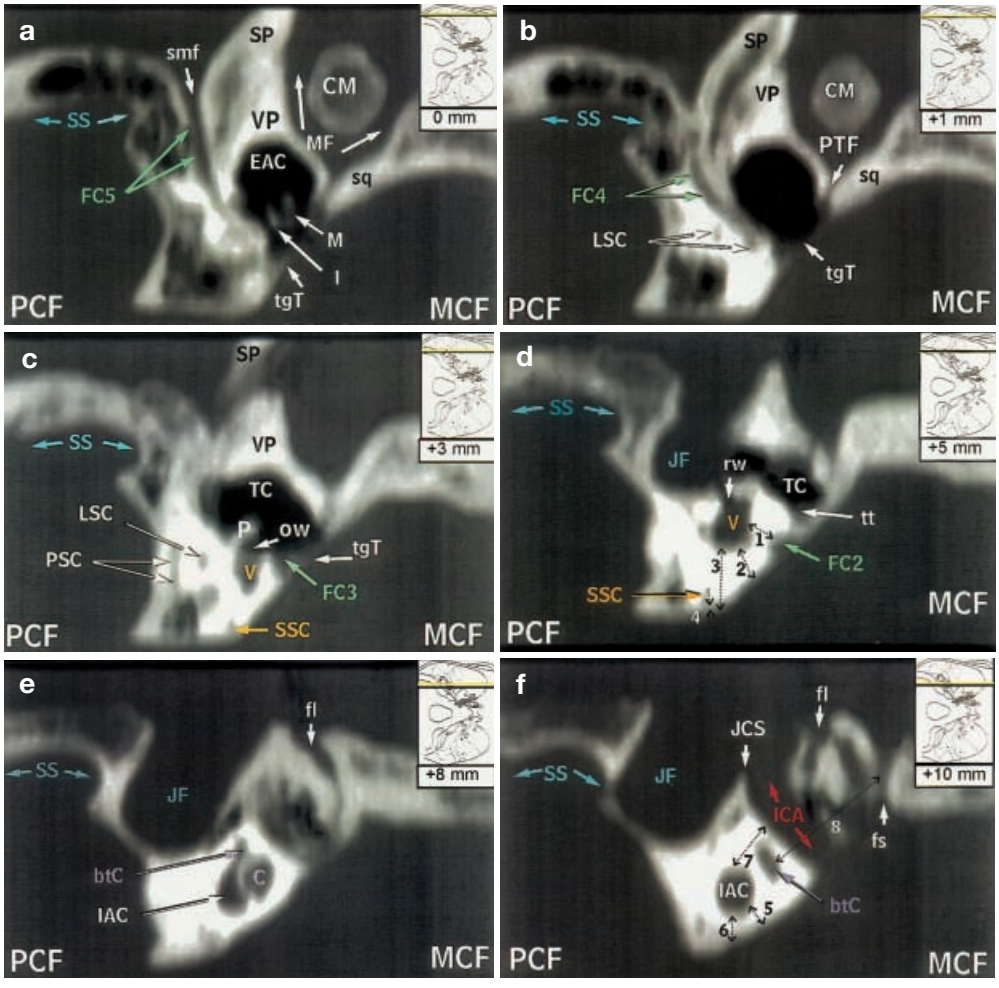

series of longitudinal sections *perpendicular* to the plane of the superior semicircular canal.

Dissection in the ITF approach is through the long axis of the petrous bone (Figs. 4, 5), so that sections along this axis are best for displaying critical anteroposterior relationships. We could find no material in the imaging literature showing temporal bone sectional anatomy in this plane. Our description should acquaint the radiologist and otologist with the complex anatomy in this radiographically novel but surgically important plane. Supplemental transverse images perpendicular to the longitudinal series (and containing the plane of the superior semicircular canal) can be created to view critical surgical landmarks in the mediolateral direction. These are dealt with in the rotated transverse atlas.

For clarity, discussion of the ITF approach is divided into four sections. The first two apply to all ITF approaches (Fig 5) and/or relationships (critical relationships 1–20, Table 2). The third describes how this approach can be customized to expose medial skull-base structures, and the fourth how it can be extended anteriorly to reach skull base pathology as far forward as the orbital apex.

The approach to the mastoid surface of the temporal bone

The surgeon sits obliquely behind the patient's head and performs a wide mastoidectomy through an extended postauricular incision. This exposes the sigmoid sinus and dura mater of the posterior and middle cranial fossae (Fig. 4).

Exposure of the facial nerve and occlusion of the sigmoid sinus

The vertical segment of the facial nerve is skeletonized (critical relationships 14 and 15, Table 2; Fig. 5). The relationship between the nerve and the jugular fossa determines the access to the hypotympanum. If the space

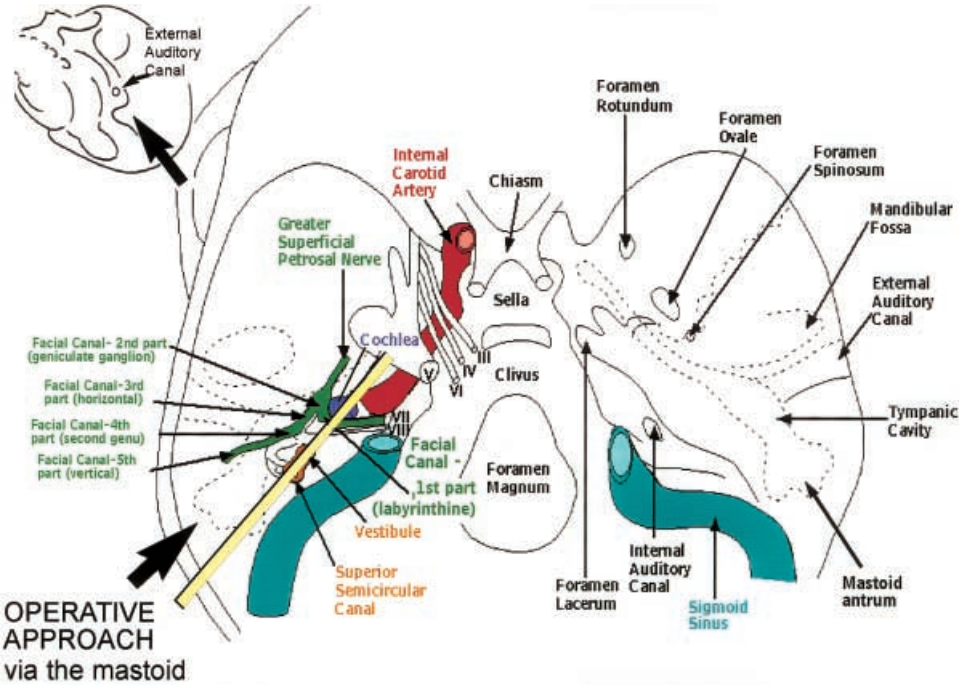

Fig. 4 Left infratemporal fossa (ITF) approach. Orientation of surgery is shown by a view from below (*left*) and a larger view from behind and above. Plane of section is marked by yellow square behind superficial petrosal nerve. To reproduce surgical perspective, longitudinal images of left side must be rotated 90 clockwise (anticlockwise for the right side) so that the sphenoid sinus is placed above the mastoid air cells (Fig. 5). (Reproduced with permission and modified from [62, 63]

Table 2 Relationships in infratemporal fossa or facial recess approaches

1	Nasopharynx to mandibular (glenoid) fossa
2	Nasopharynx to foramen ovale
3	Foramen ovale to foramen spinosum
4	Foramen spinosum to petrotympanic fissure
5	Petrotympanic fissure to external auditory canal
6	Horizontal portion of internal carotid artery to middle cranial fossa, anterior
7	Horizontal portion of internal carotid artery to middle cranial fossa, posterior
8	Internal carotid artery to basal turn of cochlea
9	Jugular fossa to basal turn of cochlea
10	Internal carotid artery to internal auditory canal
11	Jugulocarotid spine to internal auditory canal
12	Jugular fossa to fundus of internal auditory canal
13	Jugular fossa to vestibule
14	Jugular fossa to second genu of facial canal
15	Jugular fossa to second genu of facial canal (lowest)
16	Internal carotid artery to second genu of facial canal
17	Jugular fossa to sigmoid sinus
18	Cochlear aqueduct to internal auditory canal
19	Jugular fossa to porus of internal auditory canal
20	Jugular fossa to posterior cranial fossa

between the nerve and the sigmoid sinus is very narrow, the only way the hypotympanum can be approached is by mobilizing the nerve [43]. After removal of the external auditory canal, the second genu and horizontal segment of the nerve are skeletonized and the tympanic bone slowly removed, exposing the petrous carotid artery at its entrance into the skull base [8, 18, 34, 35, 37, 44] (critical relationships 8 and 16, Table 1; Fig. 5e, f). The tympanic bone is critical to unlocking the deeper anatomy of the temporal bone. A surgical mishap here may lead to inadvertent entrance into the jugular bulb, with troublesome bleeding; the petrous segment of the

Fig. 5 a–h Rotated longitudinal images of left temporal bone, projecting skull base vertically; intracranial contents lie on reader's right, sinonasal structures on the left. Numbers (*1–20*) define surgical relationships (Table 2). Abbreviations are listed below. *Insert* indicates distance from first section. **a.** This shows foramina ovale (*fo*) and spinosum (*fs*), and condyle of mandible (*CM*). **b.** Eustachian tube (*ET*) connects the nasopharynx (*NP*) and tympanic cavity (*TC*). **c.** shows superior semicircular canal (*SSC*), facial canal (*FC2*), cochlea (*C*) and internal carotid artery (*ICA*). The stapes (*S*) is barely seen, due to the window setting. **d.** Note oval window (*ow*), vestibule (*V*), and close relationship between: TC and ICA; note also C and facial canal (*FC1*). **e.** Note fundus of internal auditory canal (*IAC*), round window (*rw*), facial canal (*FC4*), and jugular fossa (*JF*). **f.** shows facial canal (*FC5*) exiting via stylomastoid foramen (*smf*) and 7 numbered surgical relationships. **g.** Temporal bone now interfaces with posterior cranial fossa (*PCF*). Note petrous apex (*PA*), petro-occipital fissure (*POF*) and clivus (*CL*). **h.** Shows IAC opening into PCF, sulcus for inferior petrosal sinus (*IPS*), and cochlear (*Ca*) and vestibular (*Va*) aqueducts. *aaA* aditus ad antrum; *btc* basal turn of cochlea; *EAC* external auditory canal; *ECF* external carotid foramen; *FC1–5* labyrinthine, geniculate fossa, horizontal, second genu and vertical portions of facial canal; *JCS* jugulocarotid spine; *LSC* lateral semicircular canal; *M* malleus; *MA* mastoid antrum; *MAC* mastorid air cells; *MCF* middle cranial fossa; *MF* mandibular (glenoid) fossa; *P* Promatory; *porus* proximal IAC; *PTF* petrotympanic fissure; *rw* round window; *Sc* scutum; *smf* stylomastoid foramen; *sp* styloid process; *SpS* Spheroid Sinus; *SS* sigmoid sinus; (see also Fig. 3)

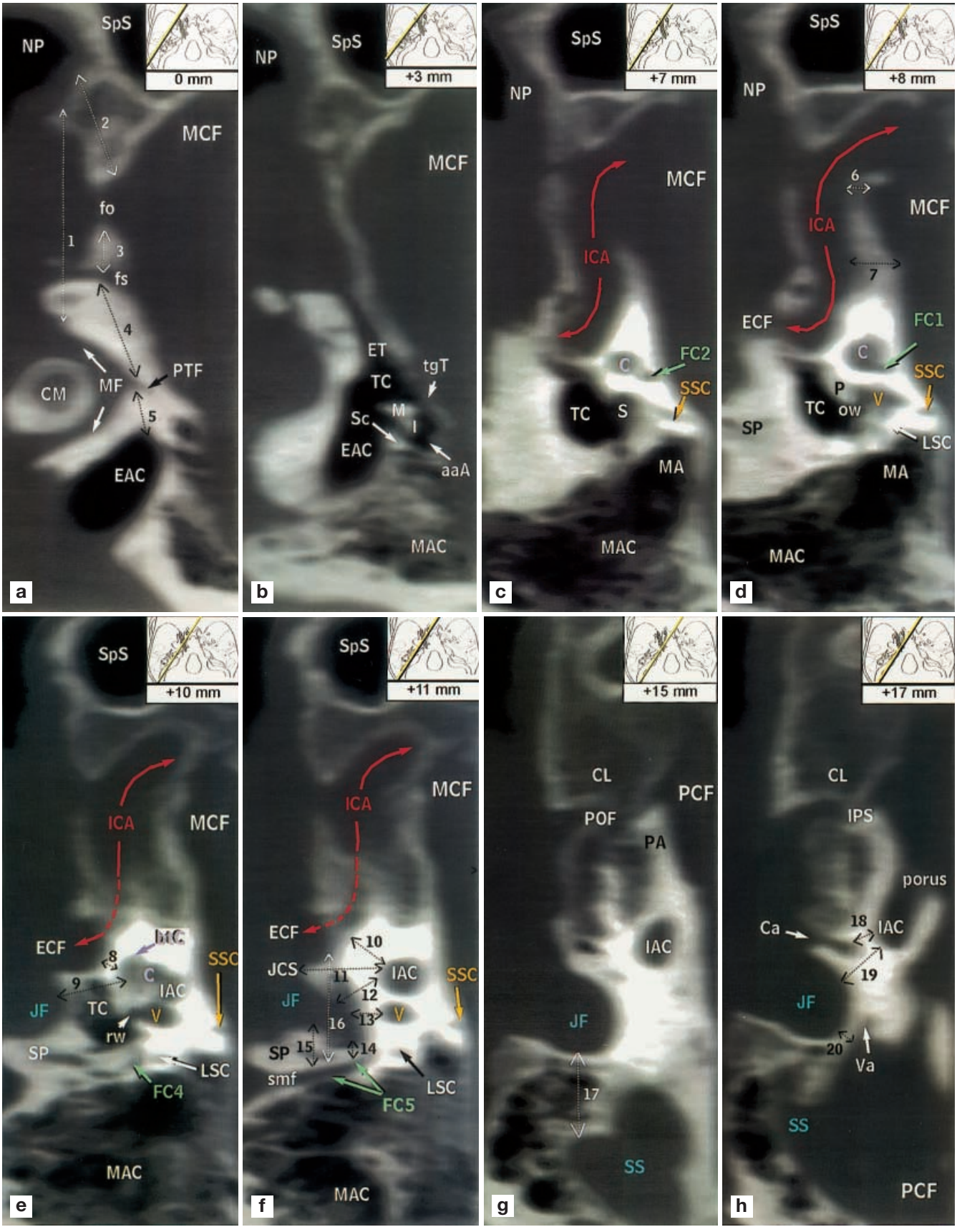
a
SpS
NP
0 mm
MCF
2
fo
1
3
fs
4
PTF
CM
MF
5
EAC
b
SpS
NP
+3 mm
MCF
ET
tgT
TC
M
Sc
I
EAC
aaA
MAC
c
SpS
NP
+7 mm
MCF
ICA
C
FC2
SSC
TC
S
MA
MAC
d
SpS
NP
+8 mm
6
MCF
ICA
7
ECF
FC1
C
SSC
P
V
TC
ow
SP
LSC
MA
MAC
e
SpS
+10 mm
ICA
MCF
ECF
bIC
8
SSC
9
C
IAC
JF
TC
V
rw
SP
LSC
FC4
MAC
f
SpS
+11 mm
ICA
MCF
ECF
10
JCS
11
IAC
SSC
JF
12
V
16
13
SP
15
14
smf
LSC
FC5
MAC
g
+15 mm
CL
PCF
POF
PA
IAC
JF
17
SS
h
+17 mm
CL
IPS
porus
Ca
18
IAC
19
JF
20
Va
SS
PCF

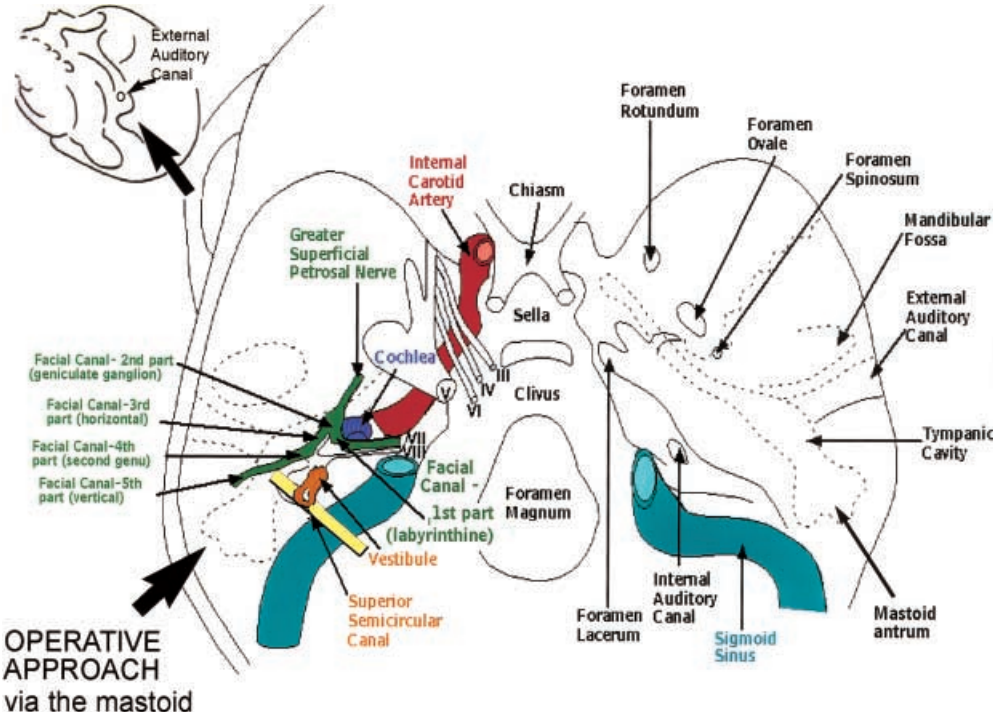

Fig. 6 Left ITF approach. Orientation of surgery is shown by a view from below (*left*) and a larger view from behind and above. Plane of section for Fig.7 is marked by yellow square behind the superior semicircular canal. To reproduce the left surgical approach the images must be rotated 90 clockwise (anticlockwise for right side) to place middle above posterior cranial fossa. (Reproduced with permission from [62, 63].

Table 3 Critical surgical relationships, infratemporal fossa approach

1	Second genu of facial canal to mid-body of external auditory canal
2	Second genu of facial canal to floor of external auditory canal
3	Jugular fossa to tympanic cavity
4	Horizontal portion of facial canal to jugular fossa
5	Maximum diameter of jugular fossa
6	Geniculate fossa segment of facial canal to basal turn of cochlea
7	Jugular fossa to basal turn of cochlea
8	Internal carotid artery to mandibular fossa
9	Internal carotid artery to basal turn of cochlea
10	Internal carotid artery to internal auditory canal
11	Jugulocarotid spine to internal auditory canal
12	Inferior petrosal sinus to internal auditory canal
13	Inferior petrosal sinus to hypoglossal canal
14	Diameter of hypoglossal canal

internal carotid artery, with catastrophic bleeding; or the cochlea, resulting in permanent hearing loss.

Next, the facial nerve is lifted out of the surgical field [45, 46]. After occlusion of the sigmoid sinus, the jugular fossa is approached rapidly to minimize bleeding from petrosal tributaries (Table 2, critical relationships 9, 12, 13, 19 and 20, Table 2; Fig. 5e–h).

Relationships to inner ear structures are most important in approaches which preserve the labyrinth and cochlea. These structures serve as a guide for extending the approach. Even in procedures which destroy the labyrinth, the approach to the internal auditory canal

Fig. 7 Rotated transverse reconstructed images of left temporal bone. ▶ Numbers (*1–14*) define surgical relationships (Table 3). Abbreviations are listed below. *Insert* indicates distance from first section. In **a** and **b**, solid yellow lines indicate bone removed for a facial recess approach, and dotted yellow lines the inferior extension. **a.** Shows stylomastoid foramen (*smf*) leading into vertical segment of facial canal (*FC5*). **b.** Body of incus (*I*) lies in epitympanic recess, bounded laterally by scutum (*Sc*). The posterior wall of the tympanic cavity is sectioned, showing facial recess (*FR*) separated from sinus tympani (*st*) by pyramidal eminence (*pe*). The facial canal (*FC4*) is difficult to identify due its thin walls and volume averaging. **c.** Note how clearly this shows surgically important dehiscence of bone between jugular fossa from tympanic cavity (relationship 3). Malleus (*M*) in tympanic cavity (*TC*) is sectioned in all three parts: head, neck, and manubrium. Crura of stapes (*S*) at oval window (*ow*) are poorly seen due to volume averaging and windowing. Round window niche (*rwn*) leads into TC; *dotted line* tympanic membrane. **d.** Note round window (*rw*), vestibule (*V*) and promontory (*P*). **e.** Labyrinthine segment of facial canal (*FC1*) leads from fundus of internal auditory canal (*IAC*) to geniculate fossa (*FC2*), matching matches the course of FC1 and FC2 in Fig 6. Note semicanal for tensor tympani (*tt*) and basal turn of cochlea (*btC*). Canal of Huguier leads from TC to mandibular fossa (*MF*). It runs in the petrotympanic fissure (*PTF*) and contains the anterior chorda tympani. **f.** Note turns of cochlea and relationship to IAC. Cochlear aqueduct (*Ca*) opens just above jugular fossa (*JF*) into posterior cranial fossa (*PCF*). **g.** IAC is sectioned through its porus. Note proximity of petrous internal carotid artery (*ICA*) and btC. Jugulocarotid spine (*JCS*) separates JF from ICA. **h.** Eustachian tube (ET) lies just above the ICA. Porus of IAC opens into PCF above the inferior petrosal sinus (*IPS*). Other abbreviations: *aaA* aditus ad antrum; *C* cochlea; *CC* common crus; *CM* condyle of mandible; *EAC* external auditory canal; *ECF* external carotid foramen; *ET* eustachian tube; *FC1–5* labyrinthine, geniculate fossa, horizontal, second genu and vertical portions of facial canal; *HC* hypoglossal canal; *IPS* inferior petrosal sinus; *MA* mastoid antrum; *MCF* middle cranial fossa; *porus* proximal IAC; *PS* Prussak's space; *PSC* posterior semicircular canal; *rwn* round window niche; *smf* stylomastoid foramen; *SP* styloid process; *sq* squamous temporal bone; *SS* sigmoid sinus; *SSC* superior semicircular canal; *tgT* tegmen tympani; *Va* vestibular aqueduct; *VP* vaginal plate

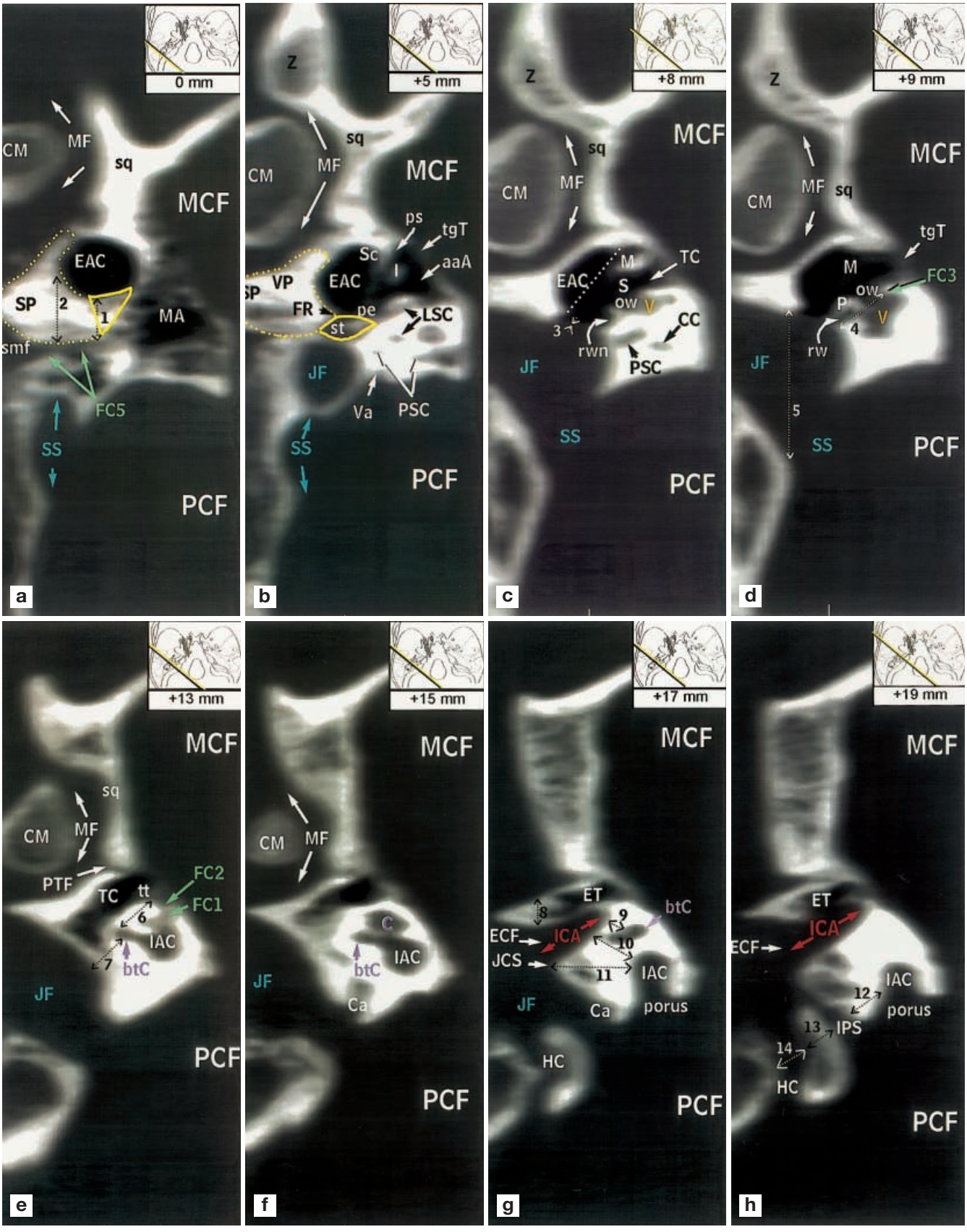
0 mm
CM
MF
sq
MCF
EAC
SP
2
1
MA
smf
FC5
SS
PCF
a
+5 mm
Z
sq
CM
MF
MCF
ps
tgT
Sc
I
aaA
VP
EAC
FR
pe
st
LSC
JF
Va
PSC
SS
PCF
b
+8 mm
Z
sq
MCF
CM
MF
M
TC
EAC
S
ow
V
3
CC
rwn
PSC
JF
SS
PCF
c
+9 mm
Z
MCF
CM
MF
sq
tgT
M
FC3
ow
P
V
4
rw
JF
5
SS
PCF
d
+13 mm
MCF
sq
CM
MF
PTF
TC
tt
FC2
FC1
6
IAC
7
btC
JF
PCF
e
+15 mm
MCF
CM
MF
C
IAC
btC
JF
Ca
PCF
f
+17 mm
MCF
ET
8
btC
ECF
ICA
9
10
JCS
11
IAC
JF
Ca
porus
HC
PCF
g
+19 mm
MCF
ET
ECF
ICA
IAC
12
porus
13
IPS
14
HC
PCF
h

from within the labyrinth is critical, because the facial nerve or anterior inferior cerebellar artery may be injured if the internal auditory canal is inadvertently entered [47].

Extensions medially (approach to the internal auditory canal through the labyrinth and/or cochlea)

Once the jugular bulb has been opened, the surgical exposure is then increased in all directions. The dura mater is delineated in the middle cranial fossa. If a tumor is large, a labyrinthectomy and cochleatectomy can be performed (translabyrinthine and transcochlear approaches) with full exposure of the internal auditory canal [48, 49, 50]. To preserve its function, the remainder of the facial nerve is rerouted out of the surgical field [34, 36, 37, 44] (critical relationships 10 and 11; Table 2, Fig 5f, h).

Extensions anteriorly

The ITF approach can be extended for wider exposure of the skull base, in what are typically designated type A, B, and C ITF approaches (not illustrated). Type A exposes the internal carotid artery in its bony canal [45, 51]; the point of entry of the internal carotid artery into the skull base is a critical landmark (critical relationship 5, Table 2; Fig 5 a). After opening the jugular fossa, the base of the jugulocarotid spine is removed, and the petrous internal carotid artery is skeletonized circumferentially by removing the bone separating the dura mater of the middle cranial fossa from the horizontal portion of the petrous internal carotid artery (critical relationships 6 and 7, Table 2; Fig. 5 d).

In type B, the mandibular fossa is removed to allow full exposure of the petrous internal carotid artery. The surgeon divides the middle meningeal artery at the foramen spinosum and the mandibular division of the trigeminal nerve at the foramen ovale, increasing the anterior exposure of the skull base [8, 40, 52] (critical relationships 3 and 4, Table 2; Fig 5 a).

The widest exposure, type C, can be used to reach pathology extending into the sphenoid sinus, nasopharynx, and orbital apex [53, 54, 55, 56] (critical relationships 1 and 2, Table 2; Fig 5 a) These relationships are critical because they give the surgeon an idea of the depth of dissection.

A rotated transverse atlas for the infratemporal fossa and facial recess (FR) approaches

The transverse plane of the petrous bone was defined as the plane containing the superior semicircular canal, as described above. The transverse images were created to display surgically meaningful relationships for both the ITF and FR approaches. They were rotated to place the middle above the posterior cranial fossa, matching the surgical perspective (Fig. 6). We chose appropriate sections (Fig. 7) and determined 14 surgically important relationships (Table 3). We used the abbreviations given in Fig 5 for labeling the HRCT reconstructions [1, 2, 3, 4, 5, 17, 19, 44, 57], and color-coding as in Fig. 1 for the surgical views (Fig. 6), and the inverted sagittal CT atlas (Fig. 7).

We describe two surgical approaches and the importance of individual reconstructed rotated transverse images (Fig. 7a–h) and relationships (1–14, Table 3).

The ITF approach

This has been described in detail above. The transverse images shown in this section are perpendicular to this dissection and can be thought of as a series showing critical mediolateral relationships as they will appear at surgery. They are a useful supplement to the longitudinal views described above. The transverse images become important when the surgeon removes the bone overlying the facial nerve from the stylomastoid foramen to the geniculate fossa so that the facial nerve can be transposed out of harm's way (critical relationships 1, 2 and 4, Table 3; Fig. 7 a, d, e). Next, the surgeon must expose and remove the sigmoid sinus and the jugular bulb (critical relationships 3, 5 and 7, Table 3; Fig. 7 c, d, e).

The relationships to the inner ear structures are most important in ITF approaches that preserve the labyrinth and cochlea. As mentioned, these structures guide resection of advanced jugular fossa tumors, which require full exposure of the internal auditory canal through a labyrinthectomy and cochleactectomy. This additional exposure requires removal of the labyrinth, transportation of the facial nerve out of the fallopian canal and exposure of the internal auditory canal. Further medial exposure can be obtained by removal of the cochlea (Table 3, critical relationships 6, 9–12, Table 3; Fig. 7 e, g, h).

Type A, B, and C approaches have already been described. The mediolateral relationship between the mandibular fossa to the petrous internal carotid artery is important in type A, since the mandibular fossa is lateral to the point at which the internal carotid artery enters the skull base (critical relationship 8, Table 3; Fig. 7). Further anterior extension (type B) can be performed to reach pathology as far forward as the cavernous sinus, clivus and hypoglossal canal (critical relationships 13 and 14, Table 3; Fig. 7 h).

The FR approach

This is used to eradicate chronic ear infection. The surgical tract created can replace the aditus ad antrum, the natural connection between the mastoid air cells and the middle ear, bypassing obstruction caused by cholesteatomas or mucosal inflammation. This approach is uniquely suitable for cochlear electrode implantation, allowing the electrode to be positioned in the round window while the implant remains in the mastoid [58].

It is a challenging maneuver in which the surgeon accesses the middle ear through the mastoid bone via the facial recess, a small triangular area outlined by a solid yellow line in Fig. 7a, b. This requires removal of the bone between the external auditory canal and the vertical segment of the facial canal. Inflammation of the mucosa within the facial recess air cells makes this approach more challenging because the visual clues which distinguish air cells from the facial nerve canal are distorted. If the facial recess is sufficiently large, the external auditory canal and tympanic membrane can be left intact, but if it is small, the surgeon must remove the first of these, in a "canal-down" procedure. Patients with well-pneumatized temporal bones tend to have a larger facial recess and are the best candidates for the facial recess approach. (critical relationships 1 and 2, Table 3; Fig. 7a). The short process of the incus (Fig. 7b) defines the location and direction of the second genu of the facial nerve which underlies this ossicle at the incudial fossa. Injury to the incus or the facial nerve results in ipsilateral deafness or facial paralysis.

The maximum exposure of a simple FR approach is shown by relationship 4 in Table 3 (Fig. 7d), which also shows the oval and round windows; the latter receives the electrode in cochlear implant surgery. In an extended FR approach, the opening is widened inferiorly to allow access to the hypotympanum (Fig. 7a, b). The external auditory canal is skeletonized inferiorly by removing the vaginal plate of the tympanic bone and the base of the styloid process. In so doing, the chorda tympani nerve (which carries taste fibers from the anterior two-thirds of the tongue) is severed in its canal [59, 60]. This extension also brings the surgeon into close proximity to the jugular bulb (which may be unusually high or dehiscent in the tympanic cavity) in the jugular fossa (critical relationship 3, Table 3; Fig 7c). This approach can be extended up to the sigmoid sinus and jugular bulb [59].

Acknowledgement We thank Carolyn Davis for her technical assistance in preparing the color illustrations.

References

1. Donaldson JA (1992) Part III. The ear. Adult anatomy. In: Donaldson JA, Duckert LG, Lambert PM, Rubel EW (eds) Surgical anatomy of the temporal bone. Raven Press, New York, pp 143–490
2. Proctor B (1989) Surgical anatomy of the ear and temporal bone. Thieme Medical, New York, pp 1–218
3. Pernkopf E (1989) Anatomy. Vol. 1: Head and neck. Urban & Schwarzenberg, Munich pp 142–192
4. Gunlock MG, Gentry LR (1998) Anatomy of the temporal bone. Neuroimaging Clin North Am 8: 195–209
5. Brogan M, Chakeres DW (1989) Computed tomography and magnetic resonance imaging of the normal anatomy of the temporal bone. Semin Ultrasound CT MR 10: 178–194
6. Maniglia AJ, Sprecher RC, Megerian CA, Lanzieri C (1992) Inferior mastoidectomy-hypotympanic approach for surgical removal of glomus jugulare tumors: an anatomical and radiologic study emphasizing distances between critical structures. Laryngoscope 102: 407–414
7. Parisier SC (1977) The middle cranial fossa approach to the internal auditory canal–an anatomical study stressing critical distances between surgical landmarks. Laryngoscope 87 [Suppl 4 Pt 2]: 1–20
8. Aslan A, Balyan FR, Taibah A, Sanna M (1998) Anatomic relationships between surgical landmarks in type b and type c infratemporal fossa approaches. Eur Arch Otorhinolaryngol 255: 259–264
9. Dew LA, Shelton C, Harnsberger HR, Thompson BG (1997) Surgical exposure of the petrous internal carotid artery: practical application for skull base surgery. Laryngoscope 107: 967–976
10. Muren C, Wadin K, Wilbrand HF (1990) The cochlea and the carotid canal. Acta Radiol 31: 33–35
11. Tomura N, Sashi R, Kobayashi M, Hirano H, Hashimoto M, Watarai J (1995) Normal variations of the temporal bone on high-resolution CT: their incidence and clinical significance. Clin Radiol 50: 144–148
12. Wadin K, Wilbrand H (1986) The topographic relations of the high jugular fossa to the inner ear. A radioanatomic investigation. Acta Radiol 27: 315–324
13. Yamakami I, Yamaura A, Ono J, Nakamura T (1996) Anatomical aspects of posterior fossa affecting lateral suboccipital approach: evaluation by bone-window CT [Japanese]. No Shinkei Geka 24: 157–163
14. Virapongse C, Sarwar M, Bhimani S, Sasaki C, Shapiro R (1985) Computed tomography of temporal bone pneumatization: 1. Normal pattern and morphology. Am J Roentgenol 145: 473–481
15. Haynes RC, Amy JR (1988) Asymmetric temporal bone pneumatization: an MR imaging pitfall. AJNR 9: 803
16. Schickinger B, Gestoettner W, Cerny C, Kornfehl J (1998) Variant petrotympanic fissure as possible cause of an otologic complication during TMJ arthroscopy. A case report. Int J Oral Maxillofac Surg 27: 17–19
17. Swartz JD, Harnsberger HR (1992) Imaging of the temporal bone. Thieme Medical, New York
18. Sick H, Veillon F (1988) Atlas of slices of the temporal bone and adjacent region. Anatomy and computed tomography. Springer-Verlag, New York, pp 108–157
19. Chakeres DW (1984) CT of ear structures: a tailored approach. Radiol Clin North Am 22: 3–14

20. Torizuka T, Hayakawa K, Satoh Y, Tanaka F, Saitoh H, Okuno Y, Ogura A, Nakayama Y, Konishi J (1992) High–resolution CT of the temporal bone: a modified baseline. Radiology 184: 109–111
21. Chakeres DW, Spiegel PK (1983) A systematic technique for comprehensive evaluation of the temporal bone by computed tomography. Radiology 146: 97–106
22. Mafee MF, Kumar A, Tahmoressi CN, et al (1988) Direct sagittal CT in the evaluation of temporal bone disease. Am J Roentgenol 150: 1403–1410
23. Dastidar P, Pertti R, Karhuketo T (1997) Axial HRCT, two-dimensional and maximum intensity projection reconstructions in temporal bone lesions. Acta Otolaryngol (Stockh) [Suppl 529]: 43–46
24. Schubert O, Sartor K, Forsting M, Reisser C (1996) Three-dimensional computed display of otosurgical operation sites by spiral CT. Neuroradiology 38: 663–668
25. Reisser C, Schubert O, Forsting M, Sartor K (1996) Anatomy of the temporal bone: detailed three-dimensional display based on image data from high-resolution helical CT: a preliminary report. Am J Otol 17: 473–479
26. Vrionis FD, Foley KT, Robertson JH, Shea JJ (1997) Use of cranial surface anatomic fiducials for interactive image-guided navigation in the temporal bone: a cadaveric study. Neurosurgery 40: 755–764
27. Helmberger RC, Mueller-Lisse UL, Helmberger TH (1998) Can coronal reformations from high-resolution axial spiral CT substitute coronal acquired images of the temporal bone? Radiology 209P: 424–425
28. Muren C, Ytterbergh C (1986) Computed tomography of temporal bone specimens. Acta Radiol 27: 645–651
29. Lee BCP, Black ML, Lamb RB, et al (1989) CT evaluation of the temporal bone ossicles by using oblique reformations: a technical note. AJNR 10: 431–433
30. Turski P, Norman D, DeGroot J, Capra R (1982) High-resolution CT of the petrous bone: direct vs. reformatted images. AJNR 3: 391–394
31. Kartush JM, Kemink JL, Graham MD (1985) The arcuate eminence. Topographic orientation in middle cranial fossa surgery. Ann Otol Rhinol Laryngol 94: 25–28
32. Lang J (1984) Clinical anatomy of the cerebellopontine angle and internal acoustic meatus. Adv Otorhinolaryngol 34: 8–24
33. Hayman LA, Hinck VC (1992) Clinical brain imaging: normal structure and functional anatomy. Mosby, St. Louis
34. Fisch U (1984) Infratemporal fossa approach for lesions in the temporal bone and base of the skull. Adv Otorhinolaryngol 34: 254–266
35. Fisch U, Fagan P, Valavanis A (1984) The infratemporal fossa approach for the lateral skull base. Otolaryngol Clin North Am 17: 513–552
36. Glasscock ME, Miller GW, Drake FD, Kanok MM (1978) Surgery of the skull base. Laryngoscope 88: 905–23
37. Hitselberger WE, House WF (1976) A system of operations for skull base tumors. Adv Neurol 15: 275–80
38. Jackson CG, Glasscock ME, McKennan KX, et al (1987) The surgical treatment of skull-base tumors with intracranial extension. Otolaryngol Head Neck Surg 96: 175–85
39. Fisch U (1978) Infratemporal fossa approach to tumours of the temporal bone and base of the skull. J Laryngol Otol 92: 949–67
40. Fisch U, Pillsbury HC (1979) Infratemporal fossa approach to lesions in the temporal bone and base of the skull. Arch Otolaryngol 105: 99–107
41. Donaldson JA (1981) Surgical anatomy of the temporal bone. In: Anon (ed) Saunders, Philadelphia, pp 306
42. Helms J (1981) Variations of the course of the facial nerve in the middle ear and mastoid. In: Samii M, Janetta PJ (eds) The cranial nerves: anatomy, pathology, pathophysiology, diagnosis, treatment. Springer, Berlin, pp 392
43. Aslan A, Falcioni M, Russo A, et al (1997) Anatomical considerations of high jugular bulb in lateral skull base surgery. J Laryngol Otol 111: 333–336
44. Brackmann DE (1987) The facial nerve in the infratemporal approach. Otolaryngol Head Neck Surg 97: 15–17
45. Leonetti JP, Smith PG, Linthicum FH (1990) The petrous carotid artery: anatomic relationships in skull base surgery. Otolaryngol Head Neck Surg 102: 3–12
46. Von Doersten PG, Jackler RK (1996) Anterior facial nerve rerouting in cranial base surgery: a comparison of three techniques. Otolaryngol Head Neck Surg 115: 82–88
47. Jackler RK (1996) Translabyrinthine approach. In: Atlas of neurotology and skull base surgery. Mosby, St. Louis, pp 26–31
48. House WF, Hitselberger WE, Horn KL (1986) The middle fossa transpetrous approach to the anterior-superior cerebellopontine angle. Am J Otol 7: 1–4
49. Pensak ML, Van Loveren H, Tew JM, Jr. (1989) The surgical anatomy and approaches to lesions of the lower basilar artery and vertebral artery union. Am J Otol 10: 351–357
50. Pensak ML, Van Loveren H, Tew JM, Jr., Keith RW (1994) Transpetrosal access to meningiomas juxtaposing the temporal bone. Laryngoscope 104: 814–820
51. Fisch U (1982) Infratemporal fossa approach for glomus tumors of the temporal bone. Ann Otol Rhinol Laryngol 91: 474–479
52. Donald PJ (1992) Combined middle fossa/infratemporal fossa surgery. The challenge of skull base tumor resection. Aorn J 55: 480–489
53. Fisch U (1983) The infratemporal fossa approach for nasopharyngeal tumors. Laryngoscope 93: 36–44
54. House WF, De la Cruz A, Hitselberger WE (1978) Surgery of the skull base: transcochlear approach to the petrous apex and clivus. Otolaryngology 86: 770–779
55. Sanna M, Mazzoni A, Saleh EA, Taibah AK, Russo A (1994) Lateral approaches to the median skull base through the petrous bone: the system of the modified transcochlear approach. J Laryngol Otol 108: 1036–1044
56. Shotton JC, Schmid S, Fisch U (1991) The infratemporal fossa approach for adenoid cystic carcinoma of the skull base and nasopharynx. Otolaryngol Clin North Am 24: 1445–1464
57. Wolff D, Bellucci RJ, Eggston AA (1957) Microscopic anatomy of the temporal bone. Waverly Press, Baltimore, pp 314–387
58. Jackler RK (1996) Cochlear implantation. In: Atlas of neurotology and skull base surgery. Mosby, St. Louis, pp 242–248
59. Reichenbach JR, Essig M, Haacke EM, et al (1998) High-resolution venography of the brain using magnetic resonance imaging. MAGMA 6: 62–69
60. Bielamowicz SA, Coker NJ, Jenkins HA, Igarashi M (1988) Surgical dimensions of the facial recess in adults and children. Arch Otolaryngol Head Neck Surg 114: 534–537
61. House WF, Shelton C (1994) The middle fossa approach. In: Brackmann DE, Shelton C, Arriaga MA (eds) Otologic surgery. Saunders, Philadelphia, pp 595–604
62. Jenkins H, Ator G (1994) Traumatic facial paralysis. In: Brackmann DE, Shelton C, Arriaga MA (eds) Otologic surgery. Saunders, pp 401–403
63. Fisch U, Mattox D (1988) Part 2: Surgical Anatomy. In: Microsurgery of the skull base. Thieme Medical, New York, pp 294